P10.7 THE IMPACT OF CLOSELY SPACED ELEVATION SCANS ON OBSERVATIONS OBTAINED USING THE NWRT PHASED ARRAY RADAR

Adam J. Smith[1] *, Pamela L. Heinselman[2], Phillip B. Chilson[1]
[1]*Atmospheric Radar Research Center and School of Meteorology, University of Oklahoma, Norman, OK*
[2]*NOAA/OAR National Severe Storms Laboratory, Norman, OK*

1. INTRODUCTION

The National Weather Radar Testbed (NWRT) Phased Array Radar (PAR) is currently being evaluated as a candidate for the next generation of U.S. operational weather radar system (Weadon et al. 2009). A full list of NWRT PAR specifications may be found in Zrnic et al. (2007). This radar has previously been shown to provide rapid temporal updates for tracking fast-evolving features (Heinselman et al. 2008). Experiments are ongoing to determine the full capabilities of this unique weather radar system (Heinselman et al. 2009).

One significant advantage of a phased array system is electronic beam steering, which allows radar beams to be directed without need for a mechanical pedestal. This capability allows for the development of scanning strategies which can be modified to adapt to individual weather events. One aspect of an adaptive scan that must be evaluated is the number and spacing of elevation angles. A minimum number of elevations is necessary to provide desired vertical detail. Radar data with insufficient detail will be difficult to analyze, leading to analysis errors or missed features. Thus, it is necessary to evaluate the required number and spacing of elevation angles, in order to obtain sufficient detail for analyzing the vertical structure of target features.

To best evaluate the use of elevation angles, it is desirable to obtain scans of an event that requires a large amount of vertical information. One such event is the heat burst, which is defined as a "localized, sudden increase in surface temperature associated with a thunderstorm, shower, or mesoscale convective system, often accompanied by extreme drying" (American Meteorological Society 2009). Heat bursts are studied infrequently in the literature, but occur often during the spring and summer in the Great Plains (Lane 2000; McPherson et al. 2008). Severe winds in excess of 45 m s^{-1} have been associated with heat bursts, potentially leading to significant property damage (MacKeen et al. 1998). Heat bursts are commonly associated with evaporating precipitation aloft, which generate downdrafts that reach the surface (Johnson 1983). Thus, to analyze these events, it is necessary to accurately detect evaporating precipitation aloft using a sufficient number of elevation angles.

During the 2009 Phased Array Radar Innovative Sensing Experiment (PARISE) (Heinselman et al. 2009), showers and thunderstorms associated with a widespread heat burst event were sampled by the NWRT PAR on 13 May 2009. Analysis of surface observations from the Oklahoma Mesonet have shown that more than 40 sites detected some form of heat burst during this evening. Furthermore, multiple heat bursts were observed during the PAR sampling period. To obtain a high degree of vertical resolution, the PAR used a customized scanning strategy that contained an unusually high number of elevation scans. This data provides a unique opportunity to study the vertical structure of precipitation that generates a heat burst. The scanning strategy can also be evaluated to improve future scanning methods for this type of weather event.

In this paper, we will provide an overview of the heat burst event, along with the PAR scanning strategy. Reflectivity, velocity and surface observations will be provided to show the current scanning capability of PAR. We will then present methods to analyze the

**Corresponding author address*: Adam J. Smith, Atmospheric Radar Research Center and School of Meteorology, 120 David Boren Dr., Suite 4636, Norman, OK 73072-7307; *e-mail: adam.j.smith-1@ou.edu.*

vertical structure of heat bursts as seen by weather radar. These methods will not be evaluated in this paper, but may be used to further analyze the mechanisms of heat burst generation, and how PAR elevation scans may be best used to scan heat bursts and similar meteorological phenomena.

2. PAR SCANNING STRATEGY

The “dense” vertical scanning strategy is designed to provide high vertical resolution when sampling events such as hailstorms or pulse thunderstorms. The basic design uses 25 elevations which are spaced to provide a vertical overlap of up to one-half beamwidth. This design provides the maximum amount of vertical detail while limiting coverage gaps between elevations. Due to the number of elevations used, the method requires a period of approximately 120 seconds to scan a continuous 90-degree sector. A 60-degree sector may also be selected to reduce the temporal scanning rate by a factor of one-third.

To provide sufficient vertical coverage for targets with varying distances from the radar, multiple scanning patterns were developed. The “near” scan (Fig. 1) is used for targets within 80 km from the radar. This pattern will provide vertical coverage up to 15 km AGL for targets with a range of at least 35 km from the radar. It also provides adequate coverage when scanning multiple targets with different ranges. A second pattern, the “far” scan (Fig. 2), is used for targets further than 80 km from the radar. The far scan spaces the elevation scans closer together, so it is also useful for providing greater vertical resolution in cases with low-topped targets that are close to the radar. Details on the elevation angles and the specifications used in each scanning pattern are provided in Tables 1 and 2.

The dense vertical sampling strategy also has the ability to run using an algorithm called Adaptive Data Signal Processing Algorithm for PAR Timely Scans, or ADAPTS (Heinselman et al. 2009). ADAPTS is an algorithm that scans a particular elevation and azimuth only if it is deemed “significant”. Locations are activated for scanning if a reflectivity threshold is achieved, or if continuity or areal coverage criteria are met. By using this algorithm, the number of scanning locations can be reduced, allowing for faster temporal updates. ADAPTS was not used to sample the 13 May 2009 heat burst event, but the algorithm is available for future studies that use the dense vertical sampling strategy.

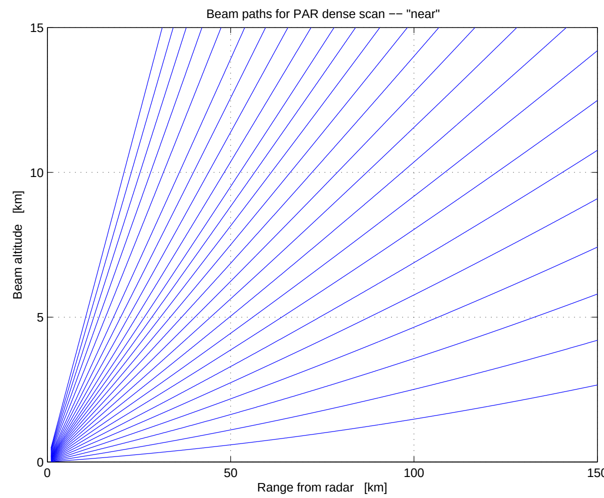

Figure 1: Beam paths in range and altitude for the dense scanning strategy – “near” scan. Additional information is presented in Table 1.

3. ANALYSIS OF THE HEAT BURST EVENT

a. Synoptic and environmental overview

A surface analysis from 0000 UTC 13 May 2009 indicates a stationary front extending north-to-south across western Nebraska and Kansas, then south-southeastward across western Oklahoma (not shown). A dryline is also present over the western Oklahoma and Texas panhandles. Temperatures ranged from near 31^{o}C in southwestern Oklahoma to 18^{o}C in far northeastern Oklahoma. High relative humidities were also present across the state.

The 0000 UTC 13 May 2009 sounding from Norman, Oklahoma (Fig. 3) shows that the region from 800 to 300 mb is relatively dry compared to the surface. This dry air indicates the potential for precipitation to evaporate aloft and generate rain-cooled downdrafts (Johnson 1983). A nearly dry-adiabatic lapse rate is also present from near 800 mb to 475 mb.

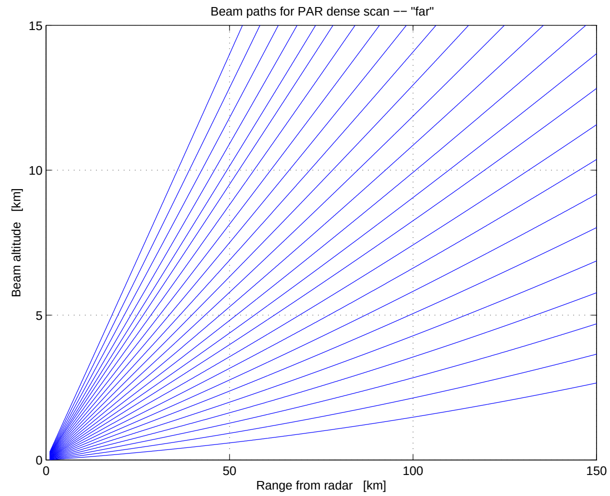

Figure 2: Same as Fig. 1, except for the "far" scan. Additional information is available in Table 2.

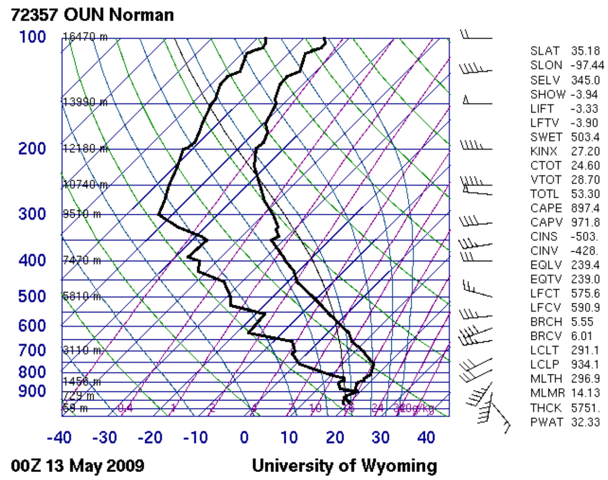

Figure 3: A sounding obtained from Norman, Oklahoma at 0000 UTC on 13 May 2009 (courtesy University of Wyoming).

This lapse rate allows the downdrafts to warm more rapidly than the environment, leading to acceleration and further evaporation. Finally, a temperature inversion, extending from the surface to approximately 800 mb, allows the descending air to overshoot its equilibrium level and reach the surface. As a result, the sounding shows that the environment is favorable for heat burst development.

Both the dryline and the stationary front were the focus for thunderstorm development, and these thunderstorms moved into western Oklahoma by 0100 UTC. Several severe wind reports were noted between 0200-0300 UTC, including a documented 70 mile per hour (31.3 m s^{-1}) wind gust at Erick, Oklahoma (Storm Prediction Center 2009). These gusts produced tree damage and also caused a semi truck to jackknife on Interstate 40 near Foss, Oklahoma. The thunderstorms then moved east-northeastward across west-central into central Oklahoma where they produced severe hail up to 2 inches (5.8 cm) in diameter. (Figs. 4–5). The storms continued to move eastward and weaken (Fig. 6), with full dissipation by 1000 UTC (Fig. 7).

b. Mesonet observations

For this study, surface observations are obtained from the Oklahoma Mesonet (McPherson et al. 2007). Observations were obtained at 5 min intervals for the period from 0200 to 1100 UTC (21:00–06:00 CDT) on 13 May 2009. For each Mesonet site, the time series of air temperature (^{o}C), dew point temperature (^{o}C) and maximum 5 min wind gusts (m s^{-1}) were scrutinized. A heat burst was identified if it satisfied the following criteria:

- A temperature increase (ΔT) of at least 1.0^{o}C over 10 min
- A simultaneous 10 min dew point increase (ΔT_d) of at least 1.0^{o}C
- A simultaneous wind gust of at least 10 m s^{-1}

Using these criteria, a total of 47 Mesonet sites observed some form of heat burst during the study period. The most significant heat burst was observed at Butler, Oklahoma, where the instruments measured ΔT = 9.1^{o}C, ΔT_d = -6.5^{o}C, and a maximum wind gust of 19.2 m s^{-1}. Wind gusts of up to 26.2 m s^{-1} were also observed with the heat bursts. These high

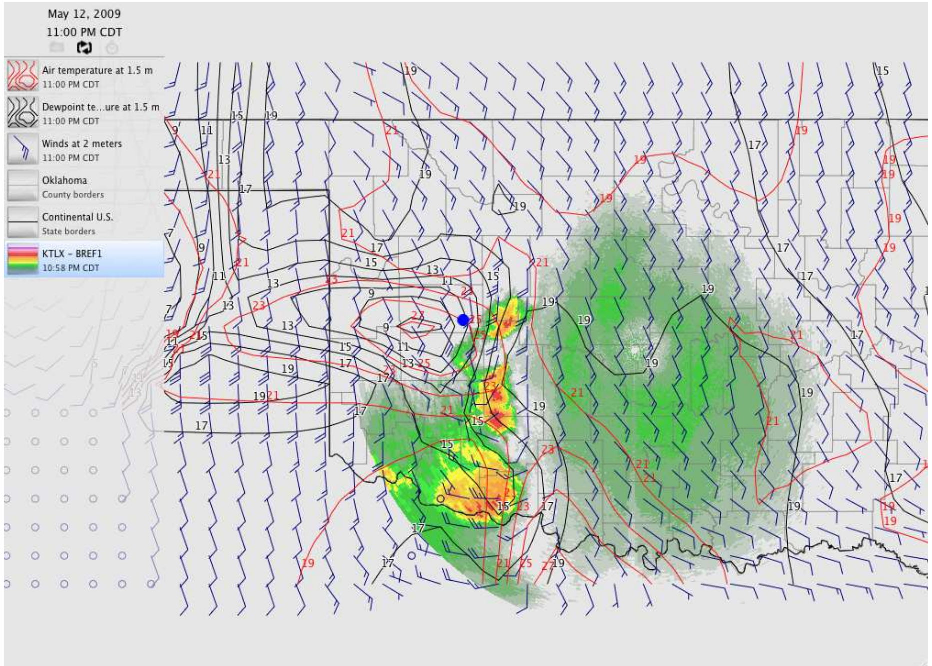

Figure 4: Regional conditions across Oklahoma at 0400 UTC (23:00 CDT). Displayed are temperature (red contours, ^{o}C), dew point (black contours, ^{o}C), wind vectors (m s^{-1}), and radar reflectivity (0.5^o elevation) from the Twin Lakes, Oklahoma WSR-88D (KTLX). For the wind barbs, short wind lines denote 2.5 m s^{-1}, while the long wind lines denote 5.0 m s^{-1}. A blue dot denotes the location of Weatherford, Oklahoma for comparison with Figs. 10–17.

winds prompted a High Wind Warning from the National Weather Service in Norman, Oklahoma. Fortunately, no wind damage was directly associated with this heat burst activity.

Figs. 4–7 track the evolution of Oklahoma Mesonet observations during the evening of 13 May 2009. Fig. 4 shows a compact region of high temperatures and low dew point temperatures over west-central Oklahoma. The area is also experiencing wind gusts of 20-30 m s^{-1}. During this time, several strong heat bursts were observed, including the strongest heat burst at Butler, Oklahoma. Strong wind gusts appear to be co-located with the region of high temperatures and low dew points. This is further evidence that heat bursts are ongoing in the region.

As the thunderstorms move eastward and begin to dissipate, heat bursts continue to occur in the wake of the precipitation. Additional weak heat bursts are observed over southwestern Oklahoma (Fig. 5), then a separate region of stronger heat bursts develops over north-central Oklahoma (Figs. 6–7). The second region appears to be associated with showers and weak thunderstorms to the southeast. However, no precipitation is apparent directly in the vicinity of the heat bursts. An analysis of WSR-88D reflectivity from Inola, Oklahoma (KINX) indicates a region of virga over the heat burst region. Thus, heat burst activity is still possible in this area, even as the area of surface precipitation moves away and vanishes.

4. RADAR ANALYSIS

During the period from 0330–0530 UTC (2230–0030 CDT), heat burst activity was sampled using the NWRT PAR and the dense vertical sampling strat-

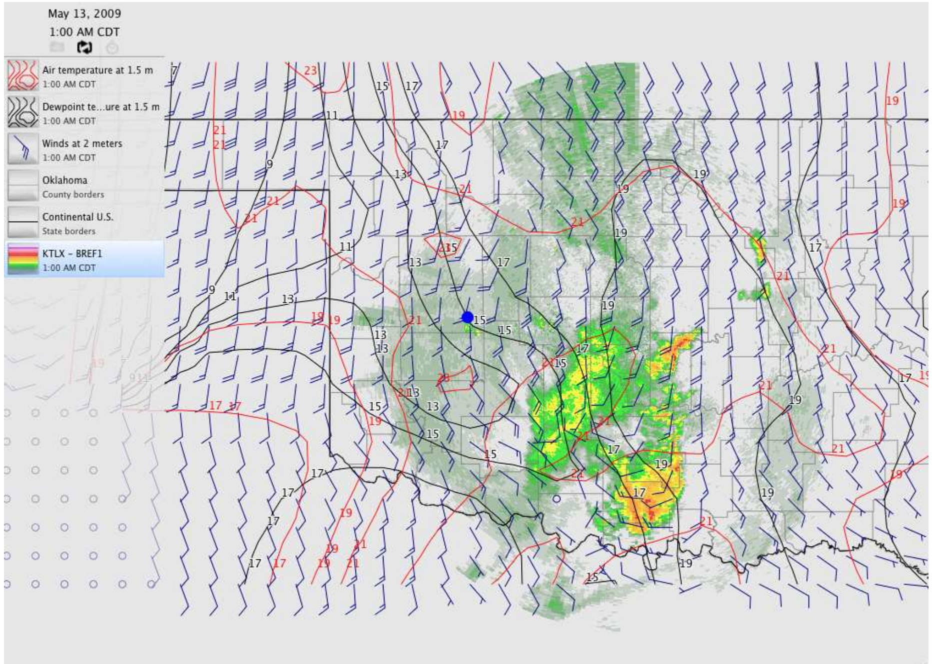

Figure 5: Same as Fig. 4, except at 0600 UTC (01:00 CDT).

egy. During the sampling period, a heat burst was observed at Weatherford, Oklahoma (Figs. 8–9). This heat burst was relatively weak when compared to other heat bursts in the region. However, the radar observations provide a unique opportunity to evaluate the conditions that may lead to heat burst development. Since the PAR scanning method is intended to provide improved vertical resolution, our discussion will focus primarily on vertical cross-sections.

To provide a benchmark for evaluating the vertical resolution obtained by PAR, we compare the PAR data with the results from the KTLX WSR-88D. During the sampling period, KTLX ran volume coverage pattern (VCP) 11, which contains 14 elevation scans. Full specifications for this VCP may be found in Federal Meteorological Handbook (2009). VCP 11 provides nearly complete vertical beam coverage, but the radar beams are not overlapped in elevation. Thus, reduced vertical resolution can be expected in KTLX scans when compared to the dense vertical sampling strategy, especially at long ranges from the radar. However, since both the PAR strategy and VCP 11 provide nearly continuous coverage in elevation, they provide a good means of comparison for this study.

Figs. 10–13 present reflectivity and velocity results from PAR and KTLX approximately 20 min prior to the heat burst event at Weatherford, Oklahoma. The cross-section is centered over Weatherford in order to evaluate the conditions that may lead to heat burst development. All vertical cross-sections are un-interpolated, in order to display the actual returns that are obtained from the radars.

Upon examining Figs. 10 and 11, it is apparent that the PAR cross-section provides a more detailed view of the storm's structure. However, the KTLX data is using super-resolution, which has a range gate width of 250 m for the lowest two tilts, and 1 km gates for the higher tilts. PAR is using a range gate width of 250 m in all elevations. While a more consistent gate width would improve KTLX resolution in range, the lack of overlapped elevations prevents the storm vertical structure from being well-resolved. Thus, it is clear that the PAR scan provides improved vertical resolution for analyzing a storm's structure. This

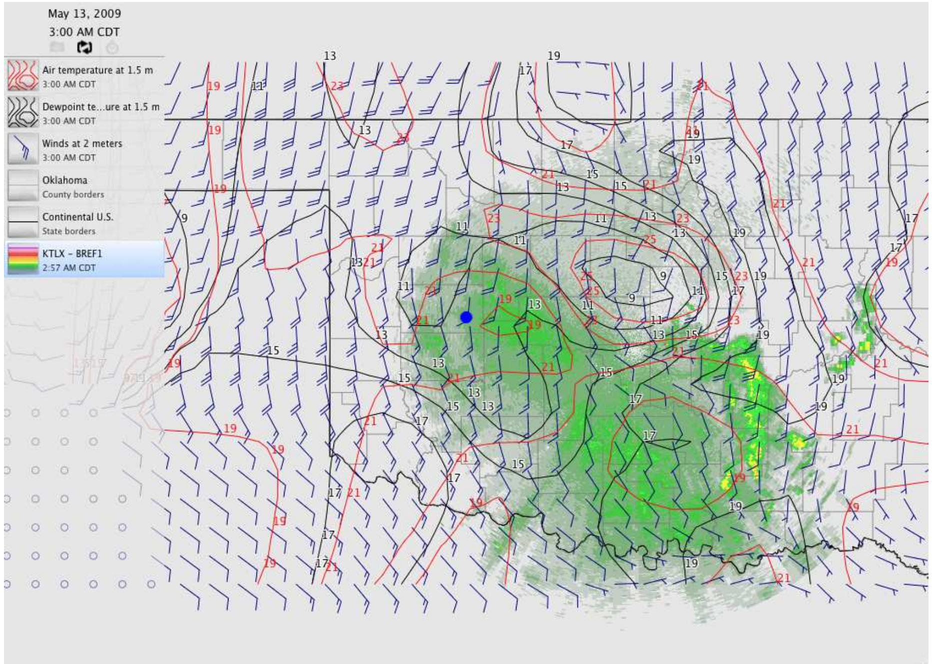

Figure 6: Same as Fig. 4, except at 0800 UTC (03:00 CDT).

capability can be critical when analyzing heat burst activity, as well as hailstorms and other events where vertical structure is important.

Figs. 12–13 provide a comparison between PAR and KTLX velocity returns. In this comparison, PAR appears to show outward velocities that extend vertically from the mid-levels to the top of the thunderstorm. This feature may indicate an updraft along with upper-level divergence. The same observations may be discerned using KTLX returns, but the features are not well resolved. As such, the improved vertical sampling on PAR appears to improve the detection of velocity features that cannot be well-observed using current scanning techniques.

In order to directly evaluate the conditions during a heat burst, we now present reflectivity and velocity images obtained during the Weatherford heat burst (Figs. 14–17). The reflectivity comparison shows an area of virga aloft as the heat burst is occurring. Mesonet observations show that no precipitation was observed during this time. Thus, these images indicate that heat burst development was likely due to evaporating virga, which generated a downdraft due to evaporational cooling. This process closely follows the mechanism discussed by Johnson (1983).

However, the two radars provide a significantly different view of the virga. KTLX does detect the precipitation aloft, but is unable to resolve the depth or details within the layer. Based on the data provided, one might estimate the virga layer to exist between 7–10 km. PAR displays a well-resolved virga layer which clearly extends across 5–10 km of altitude. It is also clear that the virga exists well behind the main thunderstorm complex to the east. While this information can also be discerned using KTLX, specific details can be difficult to obtain using the current VCP. Thus, the improved vertical resolution of the PAR data provides much more useful information for this analysis.

A comparison of velocity cross-sections (Figs. 16–17) demonstrates the importance of vertical resolution when comparing velocity fields. In this comparison, both radars detect a region of stronger negative velocities almost directly above Weatherford

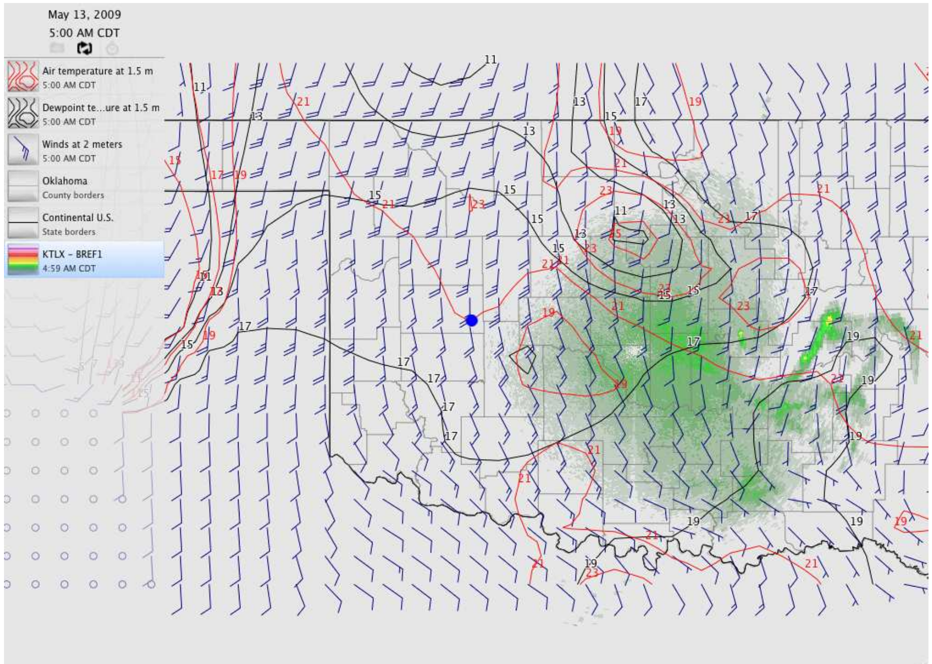

Figure 7: Same as Fig. 4, except at 1000 UTC (05:00 CDT).

(blue dot). However, PAR returns show a gradual increase in radial velocity from east to west. This result may indicate possible outflow from the precipitation to the east, which is descending toward Weatherford. KTLX does provide similar indications of increasing velocity, but there is little evidence of descent. Thus, for this case, the dense PAR sampling provides the resolution required to detect potential downdrafts. These observations are key for detecting and analyzing heat burst events.

In summary, PAR provides significantly improved detail when examining the reflectivity and velocity fields associated with a heat burst. When examining reflectivity, PAR provides a clear picture of how precipitation and virga are structured. In the case of heat bursts, it can be useful to know the depth and location of virga, in order to predict where a heat burst may occur. For velocity, improved vertical resolution can resolve small-scale features and minimal changes in radial velocity. These details can be critical for detecting downdrafts, outflow and other features that could indicate heat burst onset. As a result, a large number of elevation scans are critical for scanning heat burst events. From this study, we find that the PAR dense sampling strategy provides reasonable resolution for detecting heat bursts and associated features.

5. FUTURE ANALYSIS TECHNIQUES

In this paper, we have demonstrated the impact of a greater number of elevation scans on sampling results. However, the dense vertical sampling strategy uses an unusually large number of elevations. In many cases, it may be better to use fewer elevations, in order to improve the temporal sampling rate of the scan. Thus, it is necessary to determine the ideal number of elevations for scanning particular phenomena. To evaluate the minimum required number of elevation scans for a heat burst event, we will selectively remove elevations from a dense scan. By doing so, we effectively reduce the vertical resolution of the volume scan. By comparing the new “sparse” scan with results from the dense scan, we can evaluate the visual and quantitative impact of the reduced resolution. By examining the loss of continuity and consistency in radar features, we can determine the best number and spacing of elevations that will be required for sampling heat burst events.

Also, detailed vertical profiles of reflectivity and velocity may provide important insight into heat burst development. To better understand the effects of the virga layer, we propose obtaining vertical reflectivity profiles (VPRs) over a selected point of reference. These profiles will provide analysis on the depth and structure of a virga layer. By analyzing the profiles' slope and shape, it may be possible to correlate the profile structure with a heat burst's intensity. Then, by selectively removing elevations as discussed above, we can evaluate the changes in the VPRs due to decreased vertical resolution. The modified profiles would indicate the amount of vertical resolution required to adequately resolve the virga layer and detect key heat burst signatures.

6. ACKNOWLEDGEMENTS

This research was supported by grant #105099900 from the Cooperative Institute for Mesoscale Meteorological Studies. Mesonet analysis maps were plotted using the WeatherScope software package. The Oklahoma Mesonet and WeatherScope are trademarks of the Oklahoma Climatological Survey. Radar graphics were obtained using WDSS-II, which is a trademark of the University of Oklahoma.

References

American Meteorological Society, cited 2009: AMS glossary. [Available online at http://amsglossary.allenpress.com/glossary.].

Federal Meteorological Handbook, 2009: Doppler radar meteorological observations. Part A: System concepts, responsibilities, and procedures. Technical Report FCM-H11A-2009, Office of the Federal Coordinator for Meteorological Services and Supporting Research, Washington, DC.

Heinselman, P. L., D. L. Priegnitz, K. L. Manross, T. M. Smith, and R. W. Adams, 2008: Rapid sampling of severe storms by the national weather radar testbed phased array radar. *Wea. Forecast.*, **23**, 808–824.

Heinselman, P. L., and Coauthors, 2009: Phased array radar innovative sensing experiment. Preprints*, 34th Conference on Radar Meteorology*, Amer. Meteor. Soc., Williamsburg, VA, P6.5A.

Johnson, B. C., 1983: The heat burst of 29 May 1976. *Mon. Wea. Rev.*, **111**, 1776–1792.

Lane, J. D., 2000: *A climatology of heatbursts as detected by the Oklahoma Mesonet: October 1993 through September 1998*. M.S. thesis, School of Meteorology, University of Oklahoma, 141 pp.

MacKeen, P. L., D. L. Andra, and D. A. Morris, 1998: The 22-23 May 1996 heatburst: A severe wind event. Preprints*, 19th Conference on Severe Local Storms*, Amer. Meteor. Soc., Minneapolis, MN, P11.13.

McPherson, R. A., K. C. Crawford, J. D. Lane, and W. G. McPherson, 2008: A climatology of heatbursts as detected by the Oklahoma Mesonet. Preprints*, 17th Conf. on Applied Climatology*, Amer. Meteor. Soc., Whistler, BC, 1.4.

McPherson, R. A., and Coauthors, 2007: Statewide monitoring of the mesoscale environment: A technical update on the Oklahoma Mesonet. *J. Atmos. Ocean. Tech.*, **24**, 301–321.

Storm Prediction Center, cited 2009: NWS local storm reports. [Available online at http://www.spc.noaa.gov/climo/online/].

Weadon, M., P. Heinselman, D. Forsyth, W. E. Benner, G. S. Torok, and J. Kimpel, 2009: Multifunction phased array radar. *Bull. Amer. Meteor. Soc.*, **90**, 385–389.

Zrnic, D. S., J. F. Kimpel, D. E. Forsyth, A. Shapiro, G. Crain, R. Ferek, J. Heimmer, W. Benner, T. J. McNellis, and R. J. Vogt, 2007: Agile-beam phased array radar for weather observations. *Bull. Amer. Meteor. Soc.*, **88**, 1753–1766.

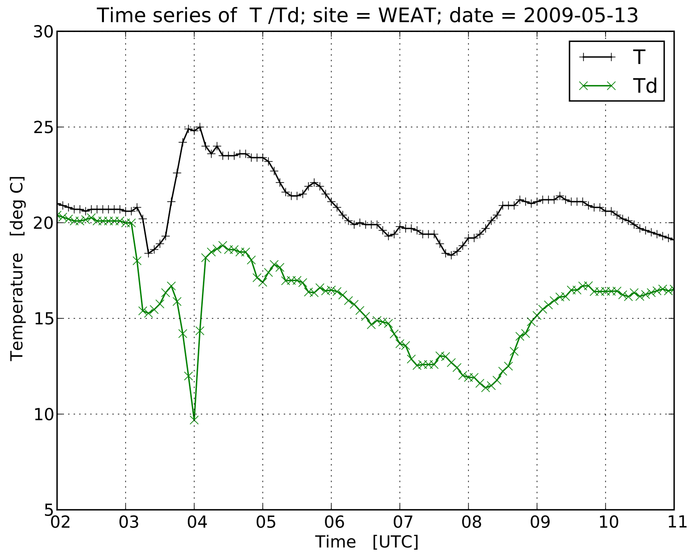

Figure 8: A time series of temperature and dew point (^{o}C) obtained from the Weatherford site (WEAT) of the Oklahoma Mesonet. The heat burst observed just before 0400 UTC corresponds with the PAR and WSR-88D data presented below.

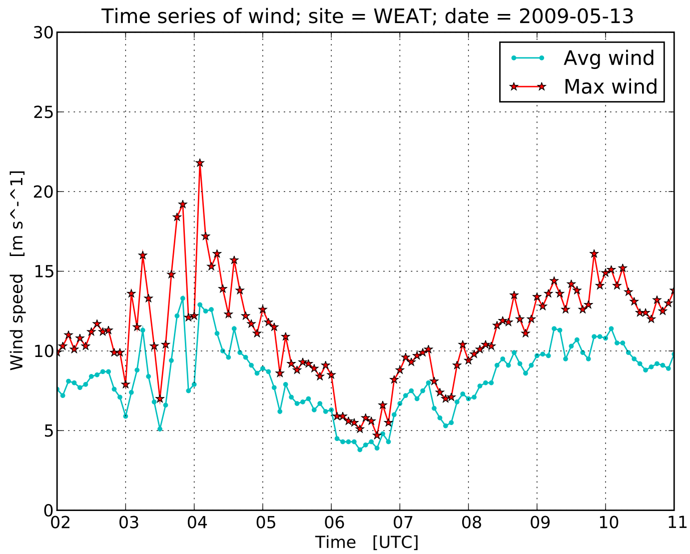

Figure 9: A time series of averaged and maximum 5 min wind speeds (m s^{-1}) obtained from the Weatherford site (WEAT) of the Oklahoma Mesonet. Prior to 0400 UTC, the observed wind gusts of near 20 m s^{-1} correspond to the heat bursts noted in Fig. 8.

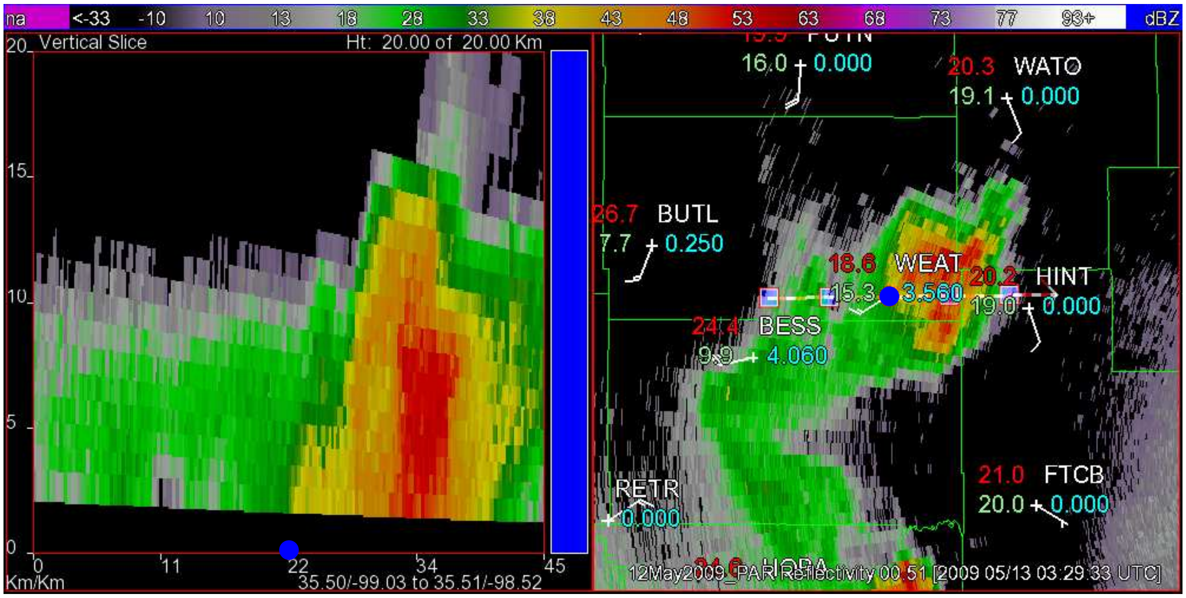

Figure 10: Reflectivity obtained from the NWRT PAR at 0329 UTC. This data was obtained using the dense sampling strategy's "far" scan. Shown are the 0.5^o elevation scan (right) and a vertical cross-section centered over Weatherford, Oklahoma (left). The blue dots denote the location of Weatherford on each panel. Oklahoma Mesonet observations are plotted on the elevation scan for reference.

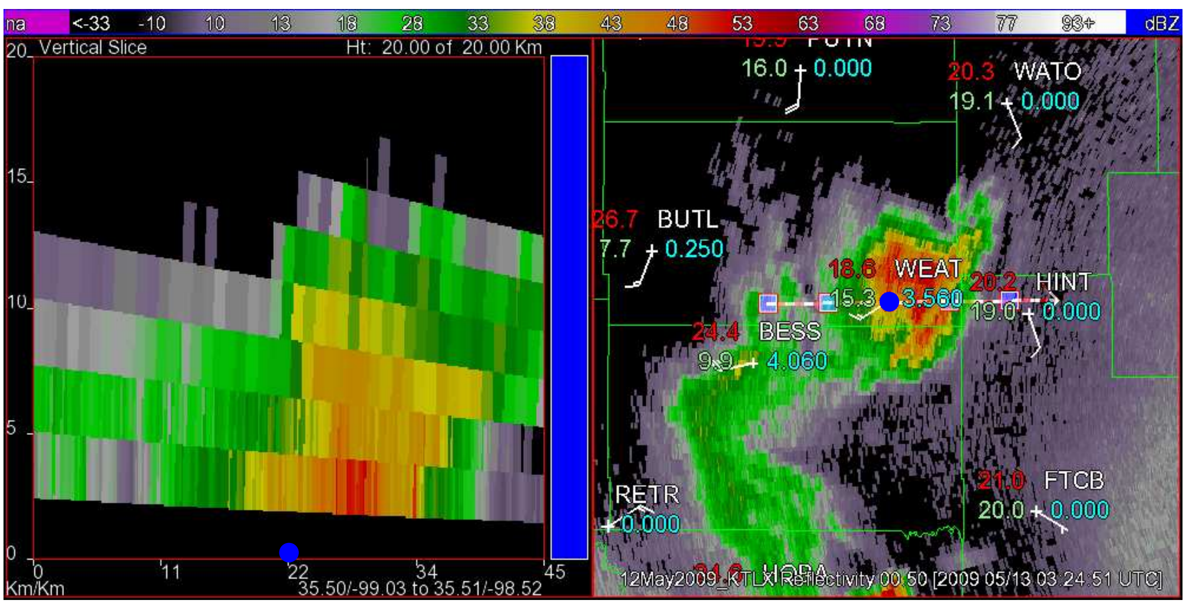

Figure 11: Reflectivity obtained from the Oklahoma City, Oklahoma WSR-88D (KTLX) at 0324 UTC. KTLX is using VCP 11, which uses 14 elevation scans. This scan is the last scan prior to obtaining the PAR data shown in Fig. 10.

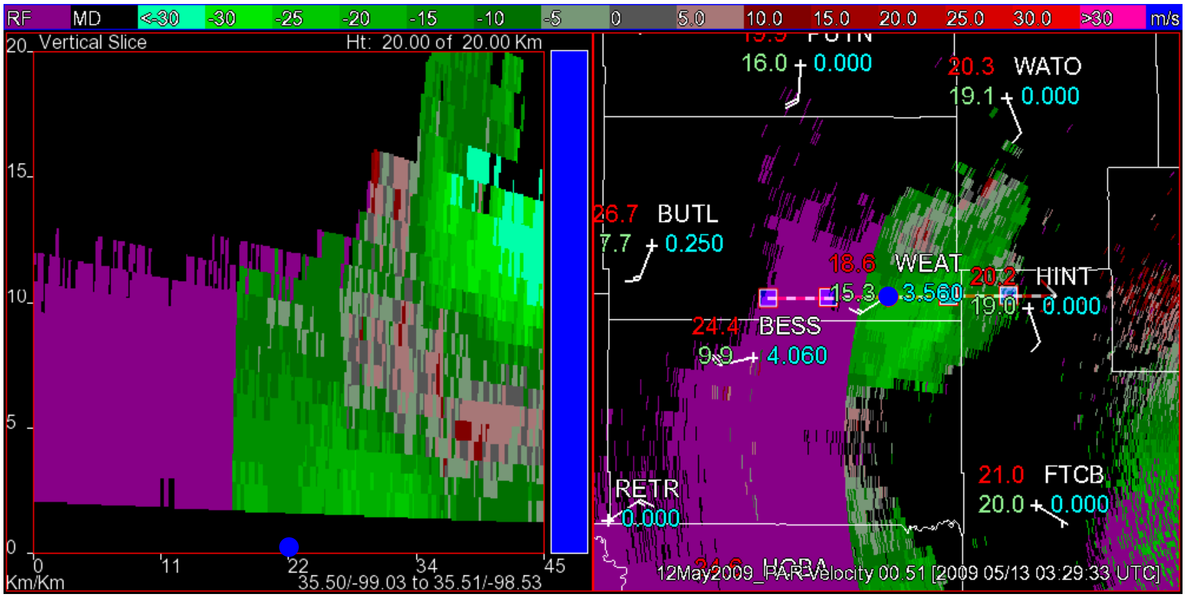

Figure 12: Radial velocity obtained by the NWRT PAR at 0329 UTC. The purple region indicates velocities that cannot be resolved due to range folding.

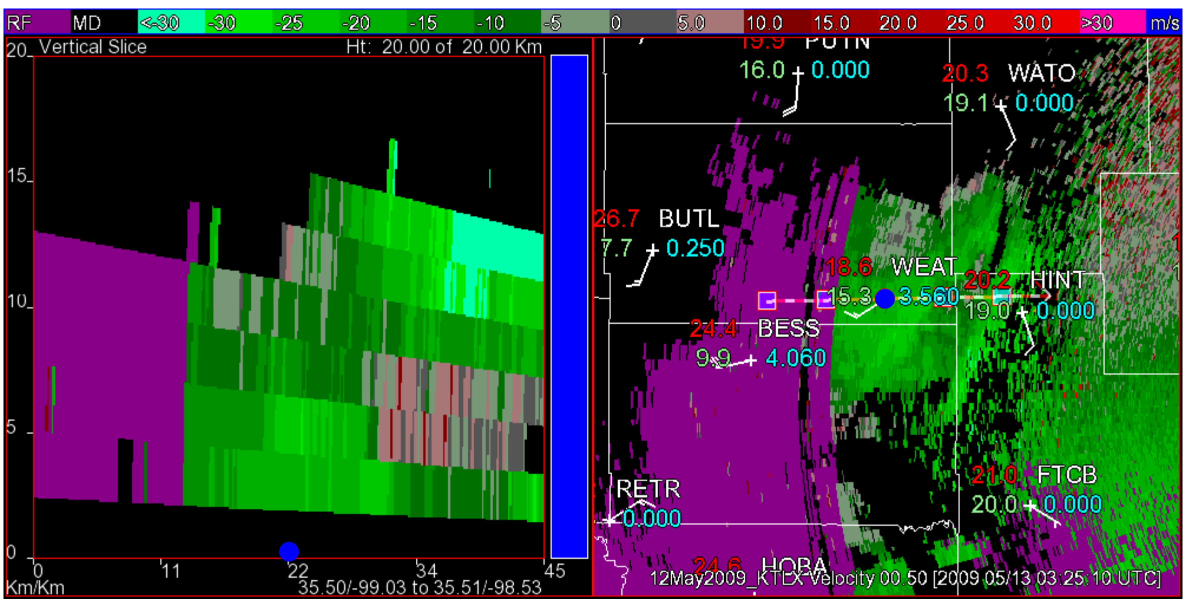

Figure 13: Radial velocity obtained by KTLX at 0325 UTC. This is the most recent KTLX scan prior to the PAR data shown in Fig. 12.

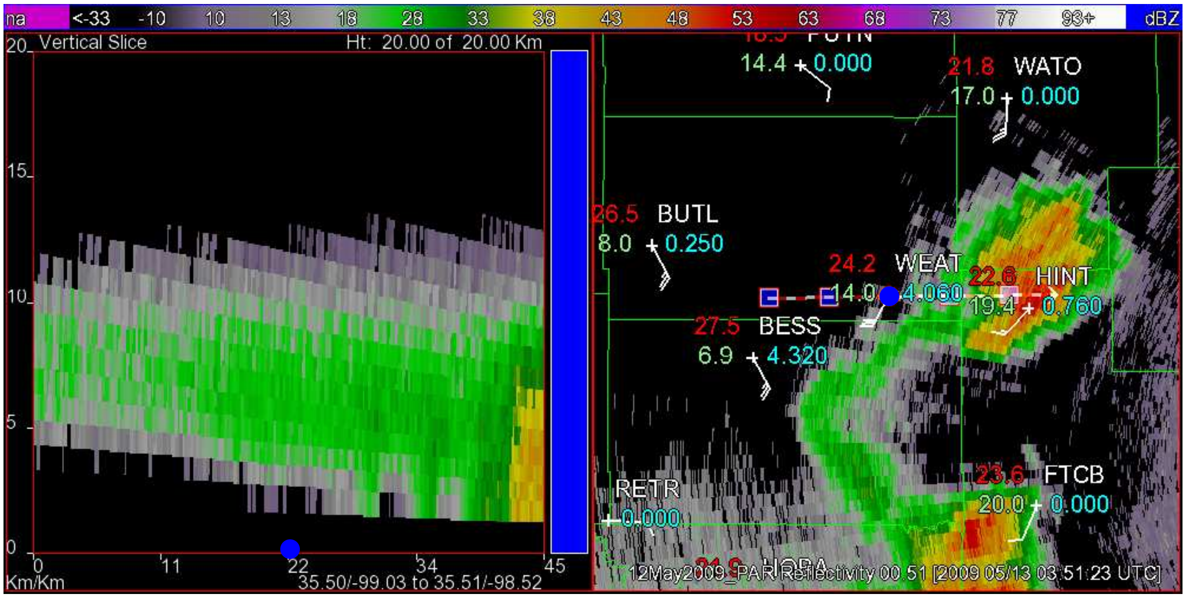

Figure 14: Same as Fig. 10, except displaying PAR reflectivity at 0351 UTC. The heat burst has now been observed at WEAT.

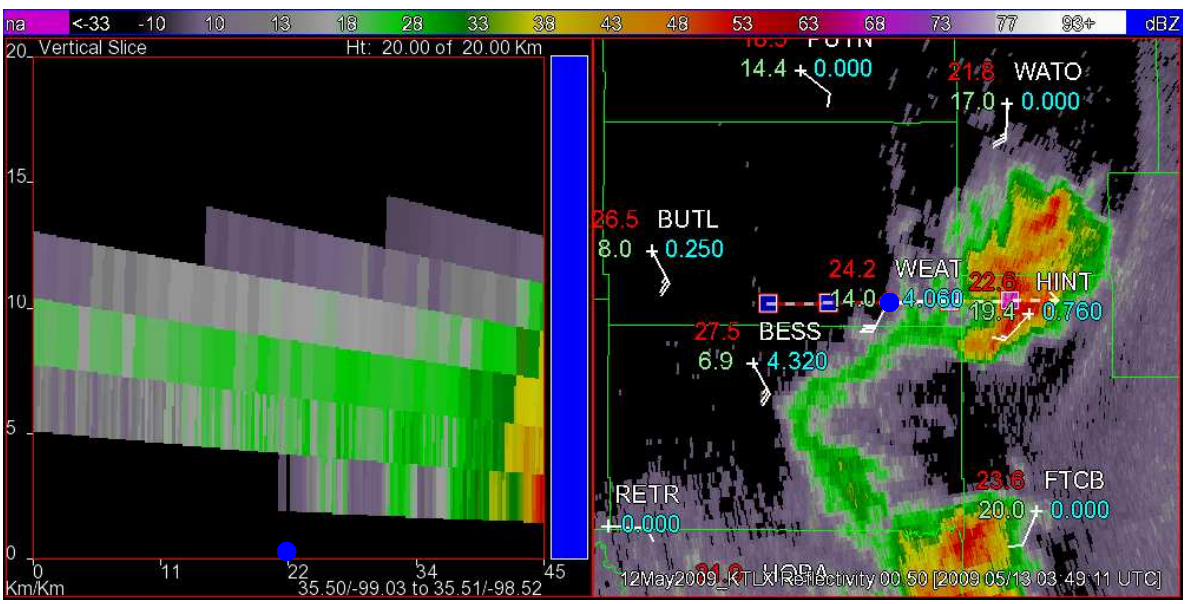

Figure 15: Same as Fig. 11, but showing KTLX reflectivity at 0349 UTC.

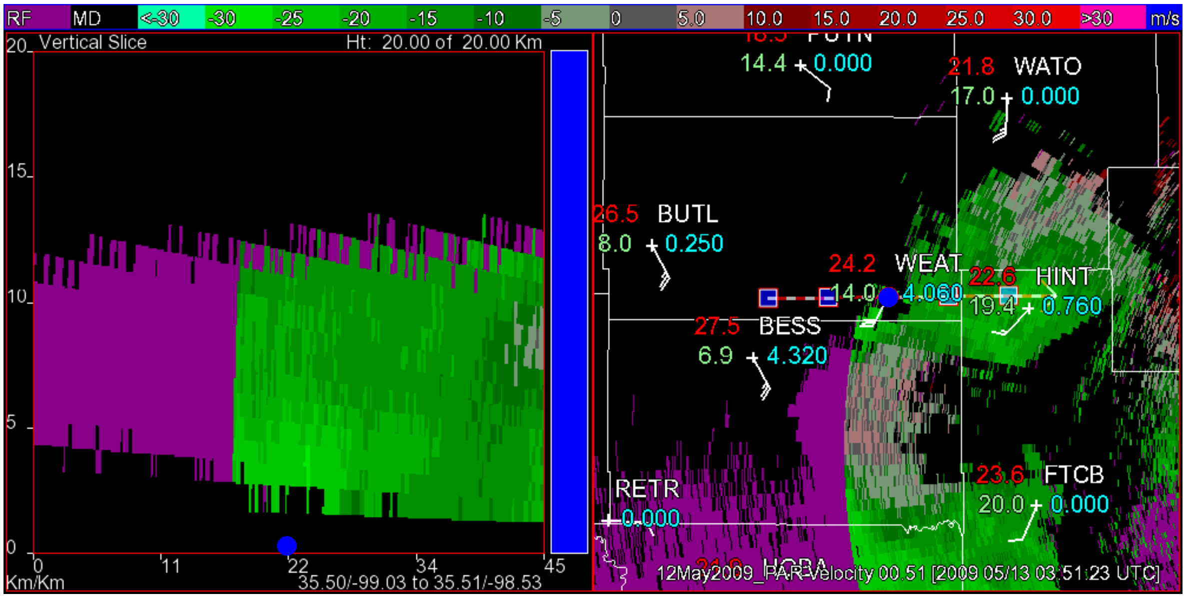

Figure 16: Same as Fig. 12, except displaying PAR radial velocity at 0351 UTC.

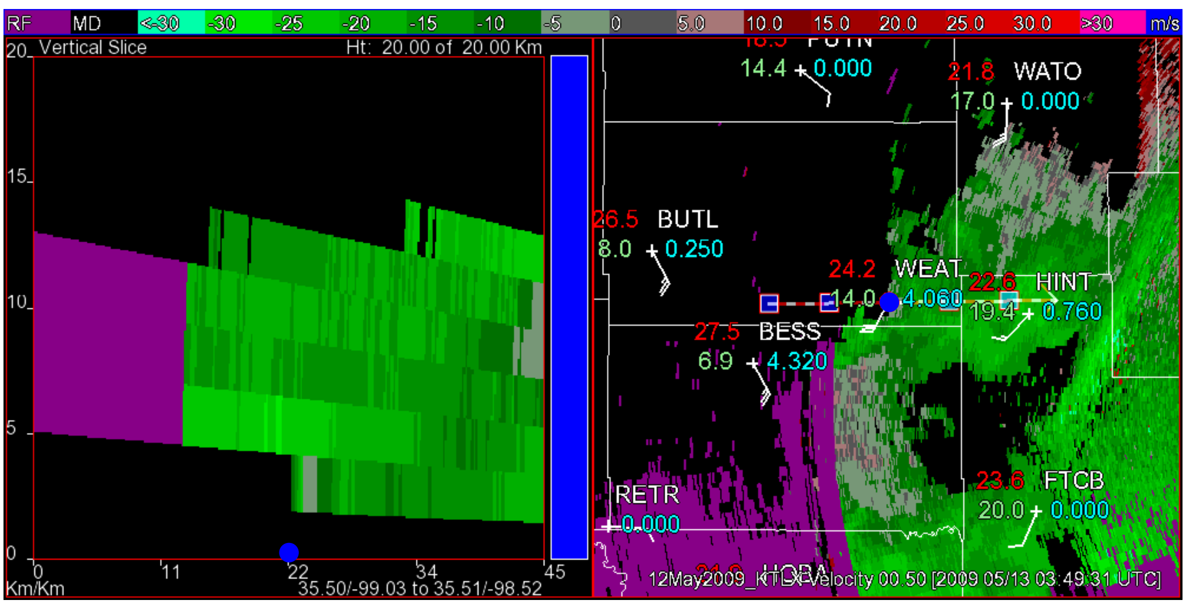

Figure 17: Same as Fig. 13, but showing KTLX radial velocity at 0349 UTC.

Table 1: Elevation angles (degrees) used for the dense scanning strategy – “near” scan. Legend: CS – Continuous Surveillance; CD – Continuous Doppler

Elevation (^{o})	Scan type	CS PRT (μs)	CS pulses (#)	CD PRT (μs)	CD pulses (#)	Nyquist vel (m s^{-1})	CS R_{max} (km)	CD R_{max} (km)
0.51	CS	3104	17				465.6	
0.51	CD			904	44	25.9		135.6
1.10	CS	3104	17				465.6	
1.10	CD			904	44	25.9		135.6
1.71	CS	2704	17				405.6	
1.71	CD			904	44	25.9		135.6
2.33	CS	2304	17				345.6	
2.33	CD			904	44	25.9		135.6
2.97	CS	2000	17				300.0	
2.97	CD			904	44	25.9		135.6
3.61	CS	1800	17				270.0	
3.61	CD			904	44	25.9		135.6
4.27	CS	1600	17				240.0	
4.27	CD			904	44	25.9		135.6
4.93	CS	1400	17				210.0	
4.93	CD			904	44	25.9		135.6
5.61	CS	1200	17				180.0	
5.61	CD			904	44	25.9		135.6
6.30	CS	1200	17				180.0	
6.30	CD			904	44	25.9		135.6
7.00	CD			904	45	25.9		135.6
7.72	CD			800	45	29.3		120.0
8.46	CD			800	45	29.3		120.0
9.22	CD			800	45	29.3		120.0
10.00	CD			800	45	29.3		120.0
10.80	CD			800	45	29.3		120.0
11.80	CD			800	45	29.3		120.0
13.00	CD			800	45	29.3		120.0
14.40	CD			800	45	29.3		120.0
16.00	CD			800	45	29.3		120.0
18.30	CD			800	45	29.3		120.0
20.70	CD			800	45	29.3		120.0
23.20	CD			800	45	29.3		120.0
25.80	CD			800	45	29.3		120.0
28.50	CD			800	45	29.3		120.0

Total scan time (60^o sector): 77.4 s
Total scan time (90^o sector): 116.2 s
Azimuth width: 1.0^o

Table 2: Elevation angles (degrees) used for the dense scanning strategy – "far" scan. Legend: CS – Continuous Surveillance; CD – Continuous Doppler

Elevation (^{o})	Scan type	CS PRT (μs)	CS pulses (#)	CD PRT (μs)	CD pulses (#)	Nyquist vel (m s^{-1})	CS R_{max} (km)	CD R_{max} (km)
0.51	CS	3104	17				465.6	
0.51	CD			904	40	25.9		135.6
0.89	CS	3104	17				465.6	
0.89	CD			904	40	25.9		135.6
1.29	CS	3000	17				450.0	
1.29	CD			904	40	25.9		135.6
1.70	CS	2704	17				405.6	
1.70	CD			904	40	25.9		135.6
2.12	CS	2504	17				375.6	
2.12	CD			904	40	25.9		135.6
2.56	CS	2200	17				330.0	
2.56	CD			904	40	25.9		135.6
3.00	CS	2000	17				300.0	
3.00	CD			904	40	25.9		135.6
3.46	CS	1800	17				270.0	
3.46	CD			904	40	25.9		135.6
3.92	CS	1648	17				247.2	
3.92	CD			904	40	25.9		135.6
4.40	CS	1504	17				225.6	
4.40	CD			904	40	25.9		135.6
4.86	CS	1400	15				210.0	
4.86	CD			904	40	25.9		135.6
5.36	CS	1304	15				195.6	
5.36	CD			904	40	25.9		135.6
5.90	CS	1200	15				180.0	
5.90	CD			904	40	25.9		135.6
6.48	CS	1048	15				157.2	
6.48	CD			904	40	25.9		135.6
7.10	CD			904	40	25.9		135.6
7.76	CD			800	40	29.3		120.0
8.46	CD			800	40	29.3		120.0
9.20	CD			800	40	29.3		120.0
9.98	CD			800	40	29.3		120.0
10.80	CD			800	40	29.3		120.0
11.54	CD			800	40	29.3		120.0
12.44	CD			800	40	29.3		120.0
13.50	CD			800	40	29.3		120.0
14.72	CD			800	40	29.3		120.0
16.10	CD			800	40	29.3		120.0

Total scan time (60^o sector):	77.4 s
Total scan time (90^o sector):	116.1 s
Azimuth width:	1.0^o